

Lawrence Berkeley National Laboratory

LBL Publications

Title

A Targeted Search for Variable Gravitationally Lensed Quasars

Permalink

<https://escholarship.org/uc/item/8gm2n5dn>

Journal

The Astrophysical Journal, 973(1)

ISSN

0004-637X

Authors

Sheu, William

Huang, Xiaosheng

Cikota, Aleksandar

et al.

Publication Date

2024-09-01

DOI

10.3847/1538-4357/ad5dad








Copyright Information

This work is made available under the terms of a Creative Commons Attribution License, available at <https://creativecommons.org/licenses/by/4.0/>

Peer reviewed



A Targeted Search for Variable Gravitationally Lensed Quasars

William Sheu^{1,2} , Xiaosheng Huang^{2,3} , Aleksandar Cikota⁴ , Nao Suzuki^{2,5} , Antonella Palmese⁶ ,
David J. Schlegel² , and Christopher Storfer^{2,7} 

¹ Department of Physics & Astronomy, University of California, Los Angeles 430 Portola Plaza, Los Angeles, CA 90095, USA; wsheu@astro.ucla.edu

² Physics Division, Lawrence Berkeley National Laboratory 1 Cyclotron Road, Berkeley, CA 94720, USA

³ Department of Physics & Astronomy, University of San Francisco 2130 Fulton Street, San Francisco, CA 94117-1080, USA

⁴ Gemini Observatory / NSF's NOIRLab Casilla 603, La Serena, Chile

⁵ Kavli Institute for the Physics and Mathematics of the Universe, University of Tokyo Kashiwa, 277-8583, Japan

⁶ Department of Physics, Carnegie Mellon University, 5000 Forbes Avenue, Pittsburgh, PA 15213-3890, USA

⁷ Institute for Astronomy, University of Hawaii, 2680 Woodlawn Drive, Honolulu, HI 96822-1897, USA

Received 2023 October 1; revised 2024 June 8; accepted 2024 June 29; published 2024 September 19

Abstract

We present a pipeline to identify photometric variability within strong gravitationally lensing candidates, in the Dark Energy Spectroscopic Instrument Legacy Imaging Surveys. In our first paper, we laid out our pipeline and presented seven new gravitationally lensed supernovae candidates in a retrospective search. In this companion paper, we apply a modified version of that pipeline to search for gravitationally lensed quasars. From a sample of 5807 strong lenses, we have identified 13 new gravitationally lensed quasar candidates (three of them quadruply lensed). We note that our methodology differs from most lensed quasar search algorithms that solely rely on the morphology, location, and color of the candidate systems. By also accounting for the temporal photometric variability of the posited lensed images in our search via difference imaging, we have discovered new lensed quasar candidates. While variability searches using difference imaging algorithms have been done in the past, they are typically performed over vast swathes of the sky, whereas we specifically target strong gravitationally lensed candidates. We also have applied our pipeline to 655 known gravitationally lensed quasar candidates from past lensed quasar searches, of which we identified 13 that display significant variability (one of them quadruply lensed). This pipeline demonstrates a promising search strategy to discover gravitationally lensed quasars in other existing and upcoming surveys.

Unified Astronomy Thesaurus concepts: [Strong gravitational lensing \(1643\)](#); [Gravitational lensing \(670\)](#); [Quasars \(1319\)](#); [Cosmology \(343\)](#); [Observational cosmology \(1146\)](#)

Materials only available in the [online version of record](#): [figure sets](#)

1. Introduction

Currently, there is a significant discrepancy between early and late universe observations of the Hubble constant (H_0), the expansion rate of the universe at the present day. Assuming a flat Λ cosmic microwave background (CMB) model, the measurement from the Planck CMB observations yields $H_0 = 67.4 \pm 0.5 \text{ km s}^{-1} \text{ Mpc}^{-1}$ (Planck Collaboration et al. 2020). On the other hand, local measurements report significantly higher values (e.g., $H_0 = 73.30 \pm 1.04 \text{ km s}^{-1} \text{ Mpc}^{-1}$; Riess et al. 2022). These predictions disagree by approximately 5σ . While recent tip-of-the-red-giant branch measurements give $H_0 = 69.8 \pm 1.7 \text{ km s}^{-1} \text{ Mpc}^{-1}$ (Freedman 2021), there remains potentially strong ambiguity with respect to the true value of H_0 .

Gravitationally lensed transients may hold the key to resolving this tension. In a strong gravitational lensing system, the light from a background galaxy is bent around a foreground galaxy, producing multiple images of the background source around the foreground lens. If the background galaxy hosts a transient event, the time delays between the images can be measured and used to constrain H_0 , when accurately modeled (e.g., Wong et al. 2019; Kelly et al. 2023). Gravitationally lensed supernovae are particularly valuable in this context due

to their well-defined light curves, and in the case of Type Ia supernovae, their standardizable peak magnitudes. However, these events are extremely rare, with only eight confirmed cases reported (Quimby et al. 2014; Kelly et al. 2015, 2022; Goobar et al. 2017, 2022; Rodney et al. 2021; Chen et al. 2022; Frye et al. 2023). In our first paper (Sheu et al. 2023, hereafter Paper I), we have identified seven new candidates for retrospective lensed supernovae using targeted image subtraction and transient detection methods applied to individual exposures of the Dark Energy Spectroscopic Instrument (DESI; DESI Collaboration et al. 2016) Legacy Imaging Surveys (Dey et al. 2019).

Compared to supernovae, quasars have stochastic light curves than lensed supernovae. However, gravitationally lensed quasars are much more common. Utilizing six quasars, Wong et al. (2019) were able to constrain H_0 with a 2.4% precision with mass profile assumptions. By expanding the current catalog of gravitationally lensed quasars, it will be possible to constrain the Hubble constant to subpercent level precision (e.g., Liao 2019), with accurate lens modeling (e.g., Shajib et al. 2023).

In addition to constraining H_0 , gravitationally lensed quasars can provide valuable insights into the properties of galaxies and quasars in the early universe, shedding light on the formation and evolution of galaxies and black holes. The gravitational lensing phenomenon itself allows for the detection of high redshift quasars, due to lens magnification. Additionally, we



Original content from this work may be used under the terms of the [Creative Commons Attribution 4.0 licence](#). Any further distribution of this work must maintain attribution to the author(s) and the title of the work, journal citation and DOI.

can achieve higher cadence and extended measurements of a quasar’s combined light curve, as there are typically two or four lensed images (e.g., Dahle et al. 2015). By leveraging spectroscopic variability, reverberation mapping of gravitationally lensed quasars also enables us to constrain the masses of black holes at high redshifts (e.g., Kelly et al. 2013).

In this paper, we show the applicability of finding new lensed quasars through a targeted difference imaging search algorithm, identifying variability within candidate systems. Specifically, we do two searches: one that identifies lensed quasar candidates in a set of strong-lens candidates via variability, and another that identifies lensed quasar candidates with strong variability in a set of previously identified lensed quasar candidates. Oftentimes in this paper, we use the word “targeted” in the sense that we focus observations on specific objects, in contrast to other search tactics that cover vast swaths of the sky to search for (lensed) quasars. Therefore if deployed in future surveys, the search utilized in this paper should be supplied with a set of lens candidates within the survey footprint and is intended to identify variable, gravitationally lensed quasar candidates from this set. While the concept of a variability search for gravitationally lensed quasars is not new (Kochanek et al. 2006) and has been deployed on previous searches with much success (e.g., Lacki et al. 2009; Kostrzewa-Rutkowska et al. 2018; Dux et al. 2023), our work is the first to deploy such a targeted difference imaging search algorithm in the DESI Legacy Imaging Surveys.

Presently there are ~ 200 confirmed gravitationally lensed quasar systems (e.g., Walsh et al. 1979; Weymann et al. 1979, 1980; Inada et al. 2012; More et al. 2015; Lemon et al. 2018a, 2018b, 2023; Agnello et al. 2018; Jaelani et al. 2021). In this paper, we present 13 new gravitationally lensed quasar candidates (three being quadruply lensed) to demonstrate our pipeline’s capability to detect lensed transients, augmenting the catalog of gravitationally lensed quasars that can be found with current data. Additionally, we confirm significant variability for 13 gravitationally lensed quasar candidates identified by Dawes et al. (2023, hereafter **D23**) and He et al. (2023, hereafter **H23**), demonstrating our pipeline’s ability to provide further confirmation for gravitationally lensed quasar candidates using existing photometric data. Follow-up spectroscopic observations of these candidates may gleam light on whether these systems are truly lensed quasars, and thus would give an estimate of our result’s accuracy.

2. Observation

We use the same observations as in Paper I. We utilize the DESI Legacy Imaging Surveys data releases (DRs) 9 and 10,⁸ specifically using observations by the Dark Energy Camera (DECam; Flaugher et al. 2015) on the 4 m Blanco telescope. These observations cover ~ 9000 deg² of the extragalactic sky below decl. $\sim 32^\circ$, across DECam g , r , i , z , and Y bands. See Figure 1 for a depiction of the Legacy Imaging Surveys DECam footprint. On average, a random point within the Legacy Imaging Surveys footprint receives 15_{-8}^{+18} observations over about five years⁹ (see Figure 2; it should be noted that oftentimes a single night captures multiple bands of a particular

pointing, and so the average total number of nights observed is lower than this).

In this paper, we first conduct a targeted search on strong-lens candidates, to find new lensed quasar candidates. As such, we compile a database of 5807 strong lenses and candidates, with the majority (about 93%) from Huang et al. (2020, 2021) and Storfer et al. (2022, hereafter SLS I, SLS II, and SLS III, respectively; shorthand for “strong-lenses search”). The remaining 7% are strong-lens candidates selected from Moustakas (2012), Carrasco et al. (2017), Diehl et al. (2017), Jacobs et al. (2017, 2019), Pourrahmani et al. (2018), Sonnenfeld & Leauthaud (2018), Wong et al. (2018) and Sonnenfeld et al. (2020). This 5807 systems sample is the same set of strong-lens targets as in Paper I.

Second, we target the 655 grade A and B lensed quasar candidates identified by **D23**¹⁰ and **H23**.¹¹ In these two papers, the candidates were discovered and graded by the morphology and location of the lensed images in the DESI Legacy Imaging Surveys. In this paper, we further examine these candidates using individual exposures in individual bands observed at different times and identify those with significant variability for all posited lensed images.

3. Methodology

We take a targeted approach to search for lensed transients, as laid out in Section 3 of Paper I. To describe succinctly, we apply two image subtraction algorithms (Bramich 2008; Hu et al. 2022) between each exposure and the median coadd across all exposures for each band, for every strong-lensing system or candidate. After generating two sets of difference images (for each difference imaging algorithm) of every exposure, we use a Python implementation (SEP; Barbary 2018) of the source extraction algorithm from Bertin & Arnouts (1996) to detect any potential sources in all difference images, with thresholds ranging from 1.0 to 2.5σ in 0.25 increments as determined by SEP (with detections $> 2.5\sigma$ treated as the same detection level as 2.5σ). Henceforth, we denote a detection in a single difference algorithm as a “subdetection” (a given transient event in a single exposure can generate two subdetections, by being detected in difference images produced by both image subtraction algorithms). All subdetections (from both subtraction algorithms, across all bands and across all exposures) are then grouped together spatially and temporally. These groupings contain all subdetections that are spatially and temporally close to other subdetections in the group. If a given group has less than three subdetections, the pipeline disregards them. If a group has three or more difference image subdetections, it is labeled as a possible transient detection. For more specificity and clarification on how we use difference imaging algorithms in our pipeline, we again refer the reader to Section 3 of Paper I.

Since we search for lensed quasars in this companion paper (in contrast to lensed supernovae in Paper I), we make the following changes to the selection criteria and apply them to our search on the strong-lens candidate sample:

⁸ <https://www.legacysurvey.org>

⁹ Derived from <https://www.legacysurvey.org/dr10/files/#random-catalogs-randoms>.

¹⁰ <https://sites.google.com/usfca.edu/neuralens/publications/lensed-qso-candidates-dawes-2022>

¹¹ https://github.com/EigenHermit/lensed_qso_cand_catalogue_He-22/blob/main/Candidates/Catalogues/H22-details.csv

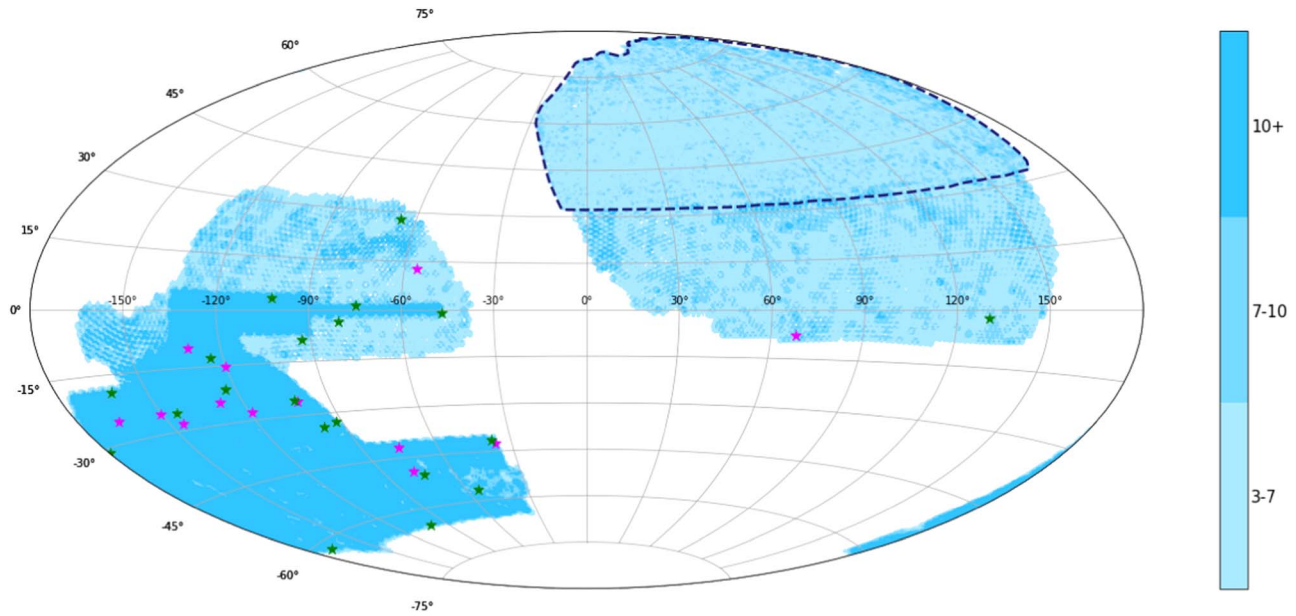


Figure 1. Legacy Imaging Surveys DR9 footprint, color coded by the z -band observation depth. The footprint of the Mayall z -band Legacy Survey and Beijing-Arizona Sky Survey is outlined in a blue dashed line, whose observations were excluded from our search. The region with 10+ exposures (bottom left) highlights the DES footprint. The green stars denote the variable lensed quasar candidates identified by our first search (targeted search on strong-lens candidates; see Section 4.1). The purple stars denote the variable lensed quasar candidates identified by our second search (targeted search on lensed quasar candidates; see Section 4.2).

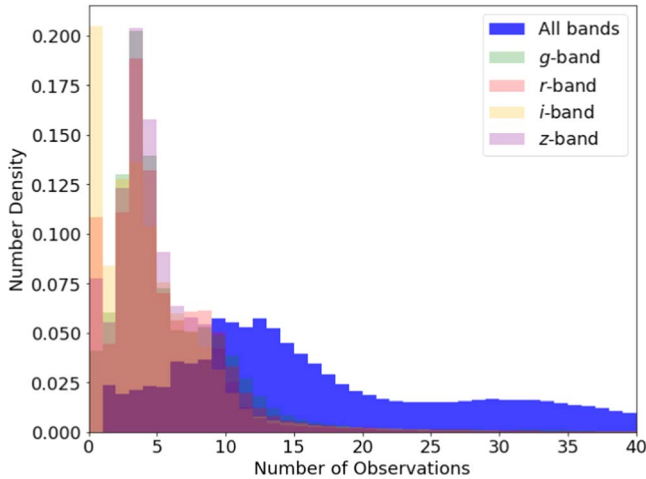


Figure 2. Histogram of the number of observations for 10^8 random points sampled from the DR10 footprint. As Y -band observations are substantially less than other bands, they are not included in this plot.

1. *Location*—The posited lensed quasar should be located at the core of the posited lensed source galaxy image (if visible), for all lensed images.
2. *Color*—The posited lensed quasar should appear blue or white in the coadded red giant branch (RGB) image (i.e., there should be significantly higher flux in the g band than in the redder bands). The lensed quasar image is usually brighter than the host galaxy, though this is not always the case. The coadded RGB images are made with the Legacy Surveys Sloan Digital Sky Survey (SDSS) RGB image generation code,¹² which weighs and assigns the g , r , i , and z bands to an associated RGB channel. While there are cases of red quasars (e.g., Fawcett et al.

2020), these are rare. All posited lensed quasar images should have similar colors.

3. *Variability*—We expect the lensed quasar to exhibit a significant level of variability between exposures. Thus, all posited lensed quasar images should display over and under subtraction between exposures. The variability should also be detected by our pipeline, and visually verified to be possible fluctuations caused by a lensed quasar (as opposed to artifacts or cosmic rays).

Note that these criteria were visually assessed by one person, and therefore are subject to human error. Of these selected lensed quasar candidates, we then compute the point-spread function (PSF) photometry of each posited image and present their light curves. A PSF must be resolved using SEP at the lensed image location; if not, we omit that exposure data from a given lensed image’s light curve. We filter out photometric data with a signal-to-noise ratio < 5 . From this, we identify 20 systems (13 new lensed quasar candidates, and seven previously identified lensed quasars). This methodology differs from other lensed quasar searches in the Legacy Imaging Surveys (e.g., D23 and H23), which solely rely on morphology (PSF-like), location, and color of identified objects. While taking these factors into account, our pipeline also relies on the photometric variability of the posited quasar images. As we will show below (see Section 4.1.2), we therefore are able to identify lensed quasar candidates previously overlooked by past searches. In addition to the targeted search, we also apply our pipeline to 655 grade A and B lensed quasar candidates identified by D23 and H23 and select candidates that show high variability for each posited lensed image. The purpose of this second search is to demonstrate the potential of utilizing targeted variability for further confirmation of lensed quasar candidates found using traditional lensed quasar search methods; thus this is not meant to be an exhaustive search. This is done, for each observed band, by setting a threshold on

¹² <https://github.com/legacysurvey/imagine/blob/main/map/views.py#L5364>

Table 1
Selection Criteria Filters

	Initial Size	Location and Color Criteria	Variability Criterion
Strong-lens Candidates Sample	5807	123 (2.12%)	20 (16.26%)
Lensed Quasar Candidates Sample	655	...	13 (1.98%)

Note. Number of candidate systems that remain after imposing specific criteria on the initial sample. The percentages shown are relative to the number of samples in the previous step.

Table 2
Lensed Quasar Candidates

System Name (1)	R.A. (deg) (2)	Decl. (deg) (3)	Prior Discovery Status (4)	Number of Observations (5)	DECam r band(mag) (6)	$\langle\bar{\sigma}\rangle$ (mag) (7)
WG021416.37-210535.3	33.5681	−21.0931	Confirmed LQ (Agnello 2018)	18/17/15/17	19.23	0.19
DESJ0340−2545	55.0363	−25.7609	Confirmed LQ (Lemon et al. 2020)	41/39/37	20.16	0.18
SDSS J2222+2745	335.5357	+27.7599	Confirmed LQ (Dahle et al. 2013)	15/15/14	20.95	0.38
KIDSJ0008−3237	2.0670	−32.6207	LQ Candidate (Khramtsov et al. 2019)	34/29/26	19.41	0.21
J0011-0845	2.8344	−8.7643	Confirmed LQ (Lemon et al. 2018b)	5/14	20.29	0.10
J0030-3358	7.6741	−33.9765	Confirmed LQ (Lemon et al. 2023)	29/22	21.01	0.14
HSCJ091843.38-022007.3	139.6802	−2.3354	Confirmed LQ (Sonnenfeld et al. 2020)	26/21	19.98	0.14
DESI-343.6329-50.4884	343.6329	−50.4884	SL Candidate (SLS III)	46/46/36	20.23	0.26
DESI-350.3458-03.5082	350.3458	−3.5082	SL Candidate (SLS III)	15/25/8	21.50	0.39
DESI-344.8782+01.2913	344.8782	+1.2913	SL Candidate (SLS III)	35/22	20.77	0.19
DESI-009.5736-64.5942	9.5736	−64.5942	SL Candidate (SLS III)	37/38	22.56	0.17
DESI-011.9124+03.3756	11.9124	+3.3756	SL Candidate (SLS III)	14/24	21.14	0.24
DESI-033.9735-12.6841	33.9735	−12.6841	SL Candidate (SLS I)	26/27	21.58	0.23
DESI-071.8595-18.9863	71.8595	−18.9863	SL Candidate (SLS III)	25/31	21.68	0.20
DESI-080.2447-61.8266	80.2447	−61.8266	SL Candidate (SLS III)	17/18	20.13	0.13
DESI-089.5700-30.9485	89.5700	−30.9485	SL Candidate (SLS II)	34/34	22.06	0.14
DESI-308.0432-41.5946	308.0432	−41.5946	SL Candidate (SLS III)	35/33	21.03	0.14
DESI-316.8445-00.9920	316.8445	−0.9920	SL Candidate (SLS II)	50/47	21.07	0.14
DESI-324.5771-56.6459	324.5771	−56.6459	SL Candidate (SLS III)	44/26	21.22	0.24
DESI-012.3074-25.6429	12.3074	−25.6429	SL Candidate (SLS III)	27	19.61	0.24
J0343-2828	55.7976	−28.4777	Disconfirmed LQ (Lemon et al. 2023)	34/34/34	20.96	0.24
DESI-011.5839-26.1241	11.5839	−26.1241	LQ Candidate (D23, H23)	32/41	20.74	0.27
DESI-029.1039-27.8562	29.1039	−27.8562	LQ Candidate (D23, H23)	30/31	19.75	0.35
DESI-030.0872-15.1609	30.0872	−15.1609	LQ Candidate (D23)	36/35	19.12	0.32
DESI-038.0655-24.4942	38.0655	−24.4942	LQ Candidate (D23, H23)	31/21	18.39	0.25
DESI-040.6886-10.0492	40.6886	−10.0492	LQ Candidate (D23, H23)	34/33	19.39	0.22
DESI-060.4504-25.2439	60.4504	−25.2439	LQ Candidate (D23)	29/24	18.74	0.28
DESI-076.5562-25.5135	76.5562	−25.5135	LQ Candidate (D23, H23)	33/34	19.87	0.17
DESI-202.0009-07.8030	202.0009	−7.8030	LQ Candidate (D23, H23)	34/24	19.75	0.23
DESI-306.7073-42.4719	306.7073	−42.4719	LQ Candidate (D23)	44/46	19.48	0.33
DESI-325.8843+12.5745	325.8843	+12.5745	LQ Candidate (D23, H23)	33/36	18.52	0.36
DESI-345.6309-41.9157	345.6309	−41.9157	LQ Candidate (D23, H23)	36/23	19.34	0.33
DESI-346.9550-49.2117	346.9550	−49.2117	LQ Candidate (D23)	44/43	20.38	0.40

Note. Summary table for our lensed quasar systems and candidates. Column (1): system name. Columns (2) and (3): R.A. and decl. of each system, respectively. Column (4): discovery status of each system and initial discovery paper, with SL and LQ referring to “strong lens” and “lensed quasar”, respectively. Column (5): number of resolved PSF photometry observations across all bands, given for each resolved image. Column (6): time-averaged DECam r -band magnitude of the brightest lensed image. Column (7): average magnitude standard deviation (Equation (1)), averaged across all resolved images and bands, as indicated by the angular brackets. The horizontal lines separate the table into three sections, corresponding to the differing discovery statuses and sections in this paper (Sections 4.1.1, 4.1.2, and 4.2, respectively). The sections are then sorted by the system’s number of observed lensed images (with the exception of DESI-344.8782+01.2913, which is thought to be quadruply lensed), then by their R.A.

their standard deviation from their mean magnitude:

$$\bar{\sigma} = \frac{1}{N} \sum_b \sqrt{N_b \sum_{m_b} (m_b - \mu_b)^2}, \quad (1)$$

where $\bar{\sigma}$ is the average magnitude standard deviation across all bands (weighted by the number of observation passes of each band), m_b is the measured PSF magnitudes for band b , μ_b is the mean PSF magnitude for band b , N_b is the total number of PSF

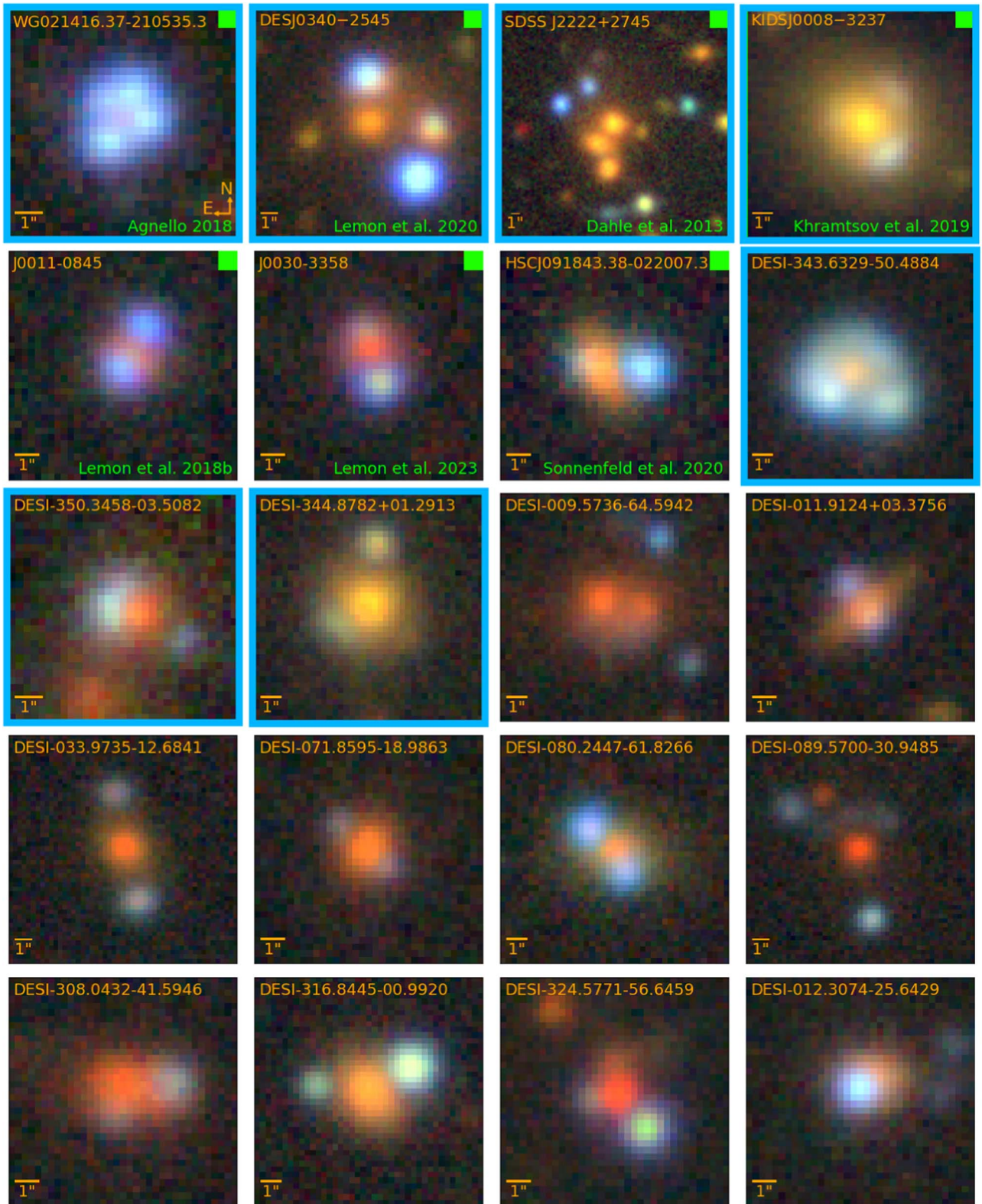


Figure 3. Our 20 identified lensed quasar candidates. The first seven are previously identified lensed quasars (with a green square at the top right corner and green text in the bottom right citing their discovery paper; all but KIDSJ0008–3237 have been spectroscopically confirmed), and the following 16 are lensed quasar candidates newly identified by our pipeline. Quadruply lensed systems are with a blue border (in the case of SDSS J2222+2745, sextuply lensed). The RGB image generation code used is discussed in Section 3.

photometry observations for band b , and N is the total number of epochs across all bands, or $\sum_b N_b$. We calculate $\bar{\sigma}$ for each image on every system, and only retain systems where all posited lensed images have a higher $\bar{\sigma}$ than twice the average

across our 20 lensed quasars and lensed quasar candidates from the first pipeline run in Section 4.1.2. We use this fiducial $\bar{\sigma}$ threshold to limit our selected candidates to ones that exhibit high variability, so as to demonstrate our pipeline’s ability to

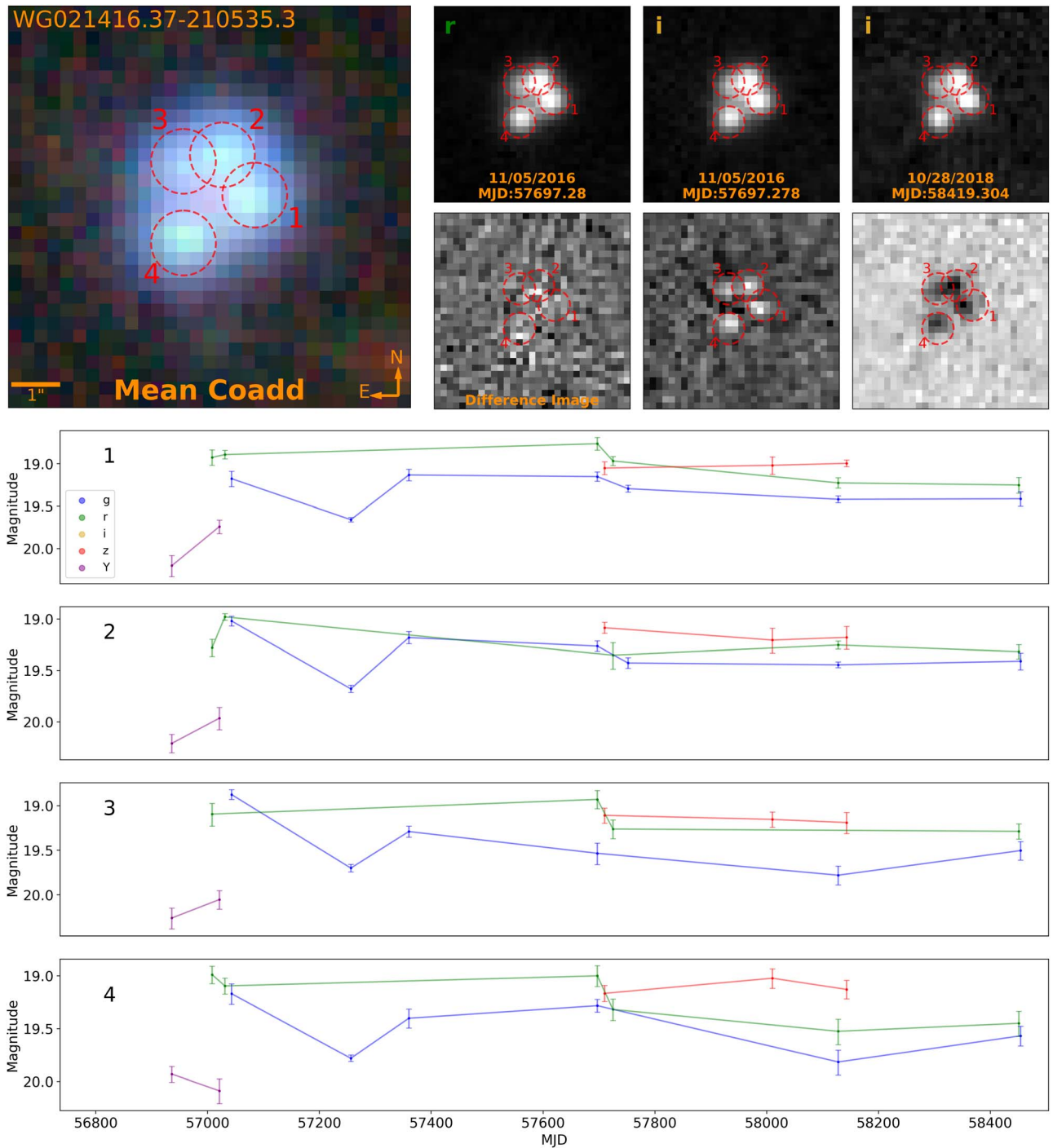


Figure 4. Lensed quasar WG021416.37-210535.3. For this and subsequent figures, we use the following formatting: the top left image is the coadded RGB image (utilizing g , r , i , and z bands), with the posited resolved lensed quasar images labeled. The RGB image generation code used is discussed in Section 3. If available, the redshift of the lens galaxy (z_L) is given below the system name; photometric measurements are given with uncertainties whereas spectroscopic measurements are shown without uncertainties. The plots to the right of the RGB image show select single-epoch exposures (top) from various bands that exhibit variability and their corresponding difference images (bottom). The bottom rows are the PSF photometry light curves of the posited images.

provide variability confirmation for already-identified lensed quasar candidates.

4. Results

In Table 1, we show how much the selection criteria filter our initial sample for the strong-lens candidates and lensed quasar candidates samples. As outlined in Section 3, for the strong-lens candidates sample, all criteria were judged via

visual inspection; for the lensed quasar candidates sample, we only apply an automated $\bar{\sigma}$ threshold set by the average of the 20 systems in the first search (as the initial sample is already filtered by a location and color criteria in D23 and H23). By comparing the “Variability Criterion” between the two samples in Table 1, we see that there is a large difference in the percentage filtered out by the criterion. This is caused by three main reasons. First, we set the fiducial $\bar{\sigma}$ threshold for the second sample to be the average of the 20

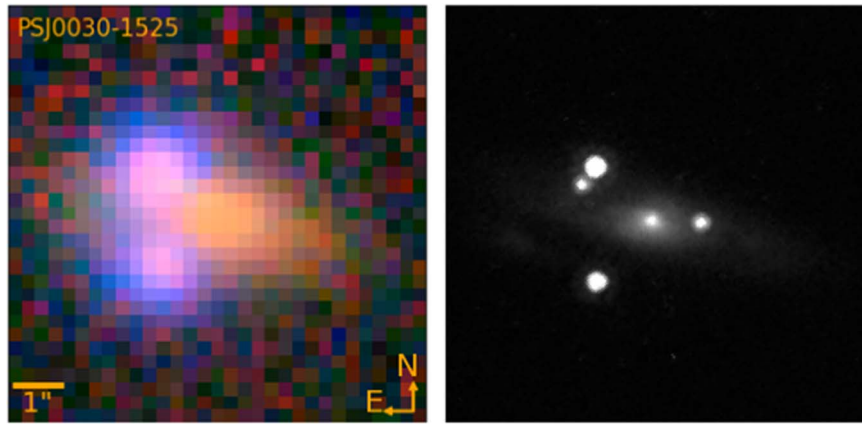


Figure 5. Side-by-side imaging of PSJ0030-1525 from the Legacy Imaging Surveys and the HST. The Legacy Surveys RGB image (utilizing the g -, r -, i -, and z -band exposures; see Section 3) is shown on the left, with the HST F814W imaging (Prop ID: 15652; PI: T. Treu) on the right. While there are only two resolved lensed quasar images from the Legacy Imaging Surveys RGB image, HST imaging reveals two additional images.

candidates found by the first, meaning that by definition, if applied to the first sample, only about half of the 20 candidates fulfill this threshold. Second, many of the systems in the lensed quasar candidates sample are cases where the quasar images are very close together but are distinguished as two separate PSF-like objects by the Tractor (a forward modeling source extraction algorithm; Lang et al. 2016). However, the difference imaging algorithms employed in this work struggle to successfully resolve these situations, and so these systems are filtered out as well. Lastly, an inherent variability bias (where quadruply lensed systems/quads are expected to have higher variability than doubly lensed systems/doubles; Lemon et al. 2020) works against the lensed quasar candidates sample, as a large majority of the D23 and H23 sample are doubly lensed quasar candidates.

We divide our results into two sections: identified lensed quasar candidates from a targeted search on strong-lens candidates (Section 4.1) and previously identified lensed quasars candidates for which we provide additional variability confirmation (Section 4.2). See Table 2 for an overview of all 33 systems. Of these, 27 systems lie within the DES footprint (see Figure 1).

Of the objects identified by the Tractor, the photometric redshifts are estimated by Zhou et al. (2020). If the Tractor is unable to deblend the lens galaxy from the lensed image(s) for a given system, then no lens redshift is provided. As many of the photometric redshifts for the lensed quasar images are not very reliable (even for confirmed lensed quasar systems), these are not presented in this paper. While we use two different difference imaging algorithms in our detection pipeline, all difference images shown in this paper are from the difference imaging algorithm of Hu et al. (2022) alone (see Section 3.2 of Paper I for our reasoning). All light-curve data presented in this paper are available here.¹³

In this discovery paper, we observe broadly coherent light-curve behavior in one or more bands, for the vast majority of the systems. The lack of coherence in a minority of our candidate’s light curves is likely due to one or more of these factors: irregularities in the exposures (oversaturation, cosmic rays, etc.), a poor signal-to-noise ratio, and/or in

the case where the lensed image is very close to the lens or other lensed images, the lens or additional lensed galaxy light causing inconsistencies in calculating photometry. Follow-up monitoring of these systems is necessary for full confirmation.

4.1. Lensed Quasar Candidates from Targeted Search

After applying our transient detection pipeline to the 5807 strong-lensing candidates, we found seven previously identified lensed quasar candidates (six of which were already spectroscopically confirmed) as well as 13 new lensed quasar candidates (with ten doubles and three quads). Figure 3 presents all 20 of these systems. The RGB image generation code used is discussed in Section 3.

4.1.1. Previously Identified Lensed Quasars

Seven systems, identified by our pipeline in our targeted search as lensed quasar candidates, were found (through a follow-up literature search) to have been previously discovered lensed quasar candidates. All but one of these seven systems (KIDSJ0008–3237) have also been spectroscopically confirmed. These systems are shown in the first seven panels of Figure 3. In this section, we present the DECam PSF photometry light curves for one lensed quasar (WG021416.37-210535.3), with the others presented in Appendix A.1.

WG021416.37-210535.3—This system is a quadruply lensed quasar (Figure 4), discovered and spectroscopically confirmed by Agnello (2018). This system was independently identified in SLS III as a strong-lens candidate, and therefore it was included in our search. We subsequently found that this is a known system. Though this system was previously discovered, here we show new photometry for this system.

4.1.2. New Lensed Quasar Candidates

In this subsection, we present the DECam PSF photometry light curves for one new lensed quasar candidate (DESI-350.3458-03.5082), with the other candidates presented in Appendix A.2.

We also note that while we present three new quad and ten new double candidates, it is anticipated that one or more of these doubles candidates are actually quadruply imaged, but only two images can be source extracted from the DECam data

¹³ <https://portal.nersc.gov/cfs/deepsrch/lquasars/>

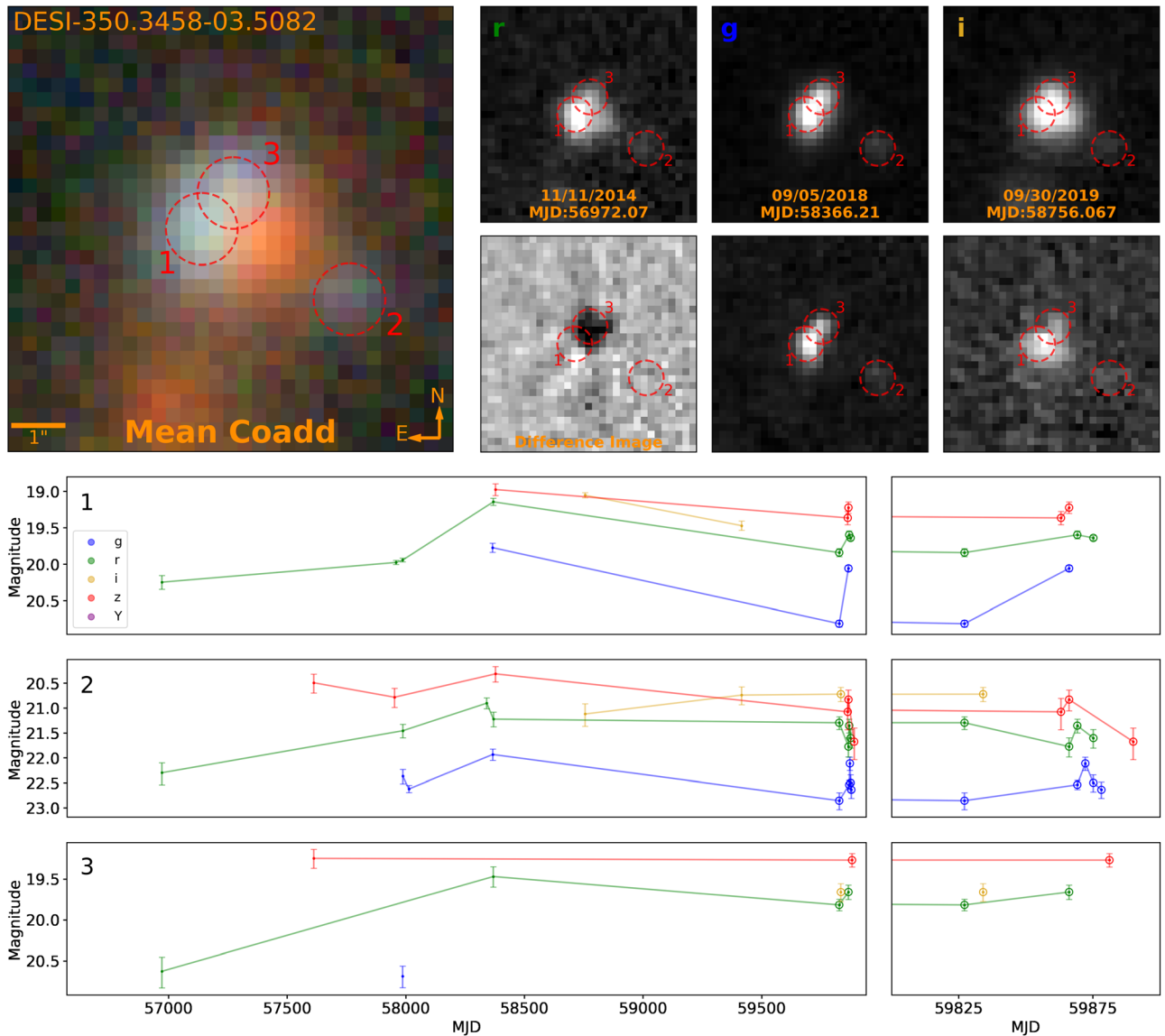


Figure 6. New lensed quasar candidate DESI-350.3458-03.5082 (see caption of Figure 4 for the full description of each subplot). This figure also displays zoomed-in panels of the light curves to the right of the light curves, in order to highlight recent follow-up observation data from 2022B-297190 (in open data points).

in the Legacy Imaging Surveys. See Figure 5 for an example such a quadruply lensed quasar system.

DESI-350.3458-03.5082—This system is a quadruply lensed quasar candidate (Figure 6), with three lensed images comprising the eastward arc and the counterimage located west of the lens galaxy. DESI-350.3458-03.5082 was initially identified as a grade B strong-lensing candidate in SLS III. In addition to the variability detected in the Legacy Imaging Surveys presented in this paper, Pan-STARRS data provide additional evidence for variability (C. Storer 2024, private communication). Without having done variability analysis, this system would have been mistaken as simply a galaxy-galaxy lensing system that displays a typical arc-counterarc configuration. For this system, recent follow-up DECam observations in the *g*, *r*, *i*, and *z* bands were analyzed (NOAO Prop ID: 2022B-297190; co-PIs: A. Palmese and L. Wang), where the variability further supports the identity of this system being a strongly lensed quasar system.

4.2. Variability Confirmation of Previously Discovered Lensed Quasar Candidates

The following 13 systems in Figure 7 are lensed quasar candidates discovered by D23 and/or H23, where our pipeline has identified significant variability within the DESI Legacy Imaging Surveys. In this section, we present the DECam PSF photometry light curves for one candidate (J0343-2828), with the other candidates presented in Appendix B. In D23 and H23, the 655 grade A and B lensed quasar candidates were selected using location- and color-based algorithms to identify close pairs/groups of PSF-like objects. Our paper provides variability confirmation for 13 of these systems, one of which is a posited quadruply lensed quasar. Our findings do not imply that all other candidates from D23 and H23 not identified by our pipeline are not lensed quasars. Variability detection depends on many factors, such as the activity of the quasar, the timing/cadence of exposures, and the time delays. Especially, the Legacy Imaging Surveys is not designed to detect transients; as shown in Section 2, the average

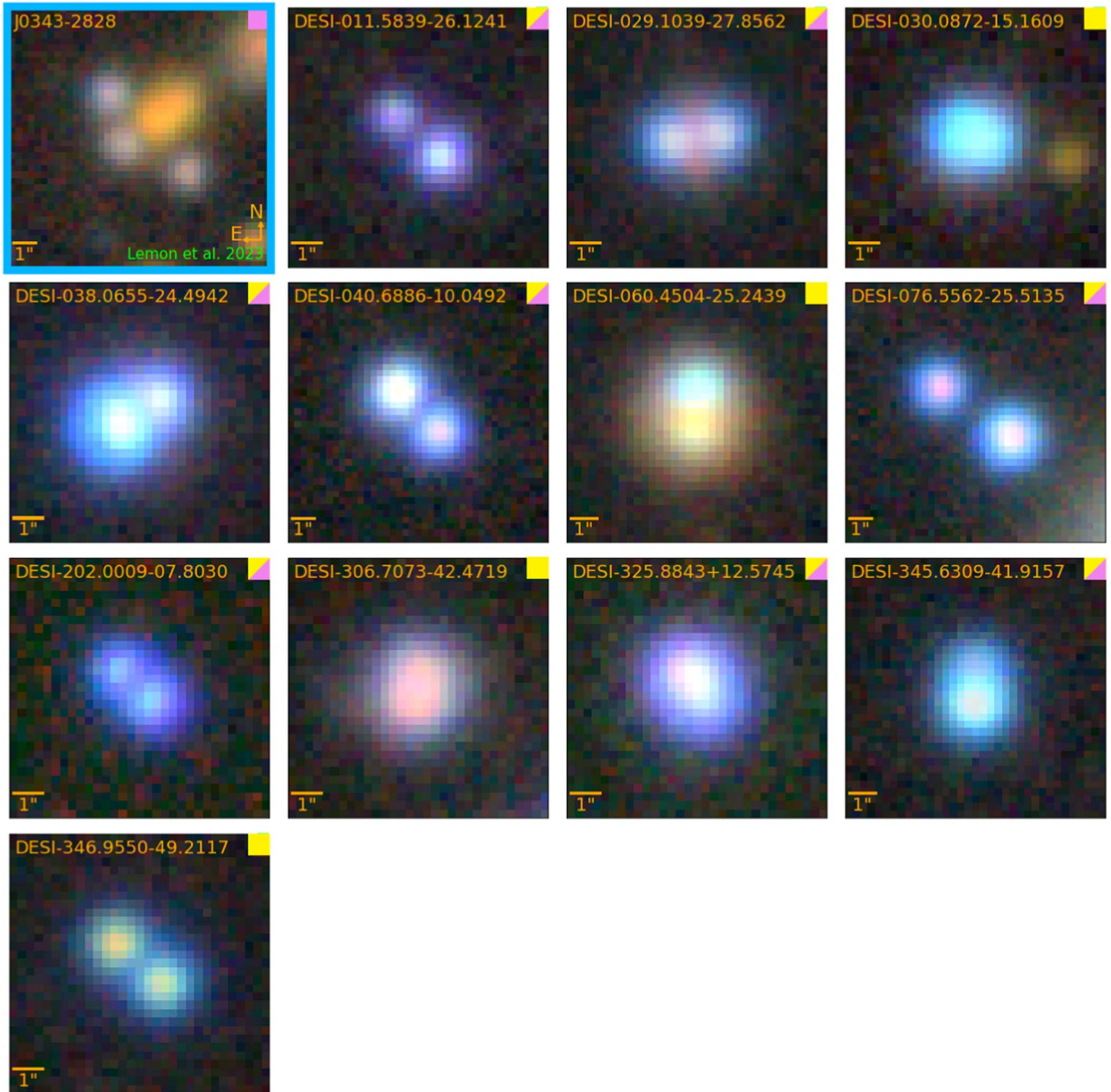


Figure 7. Our 13 previously identified lensed quasar candidates (one quad, with a blue border), for which our pipeline detects significant variability within all posited lensed quasar images. Systems with a yellow and/or magenta square on the upper right of the image are systems identified as lensed quasar candidates by D23 and/or H23, respectively. In the case of J0343-2828 (top left), the system was identified and disconfirmed as a lensed quasar candidate in Lemon et al. (2023).

cadence is approximately 100 days. As our intention is to demonstrate the viability of our methodology (detecting variability in survey data), we select the candidates where our pipeline most confidently identifies variability.

J0343-2828—This system is a quadruply lensed quasar candidate (Figure 8). J0343-2828 was initially identified as a grade A strong-lensing candidate in SLS II (named DESI-055.7976-28.4777) and then as a lensed quasar candidate in H23. Three posited lensed images are visible, and a faint fourth image is on the opposite side of the two lensed galaxies. Additional Hubble Space Telescope (HST; Prop ID: 15652; PI: T. Treu) imaging reveals an even-fainter fifth image in between the two lenses (see Figure 9). We observe significant, and broadly coherent, variability in the three brightest images, as presented in Figure 8.

A literature search shows that this system was also independently identified as a lensed quasar candidate using Gaia DR2 PSF identification in Lemon et al. (2023). However, in their work, they also presented evidence against this being a lensed quasar system: (1) the follow-up HST imaging of the system does not show diffraction patterns, and (2) spectroscopic observations do not reveal any prominent QSO emission lines.

In regard to the first point, while clear diffraction spikes are not present in the F475X and F814W bands, they are visible in the F160W band (as shown in Figure 9). This alone does not mean it is a point source; it is possible that the object is barely resolved in the optical but within the diffraction limit in the IR. However, Schmidt et al. (2023) modeled the system well with a PSF light profile in the source plane across all three HST bands, which gives additional credence to the lensed quasar hypothesis.

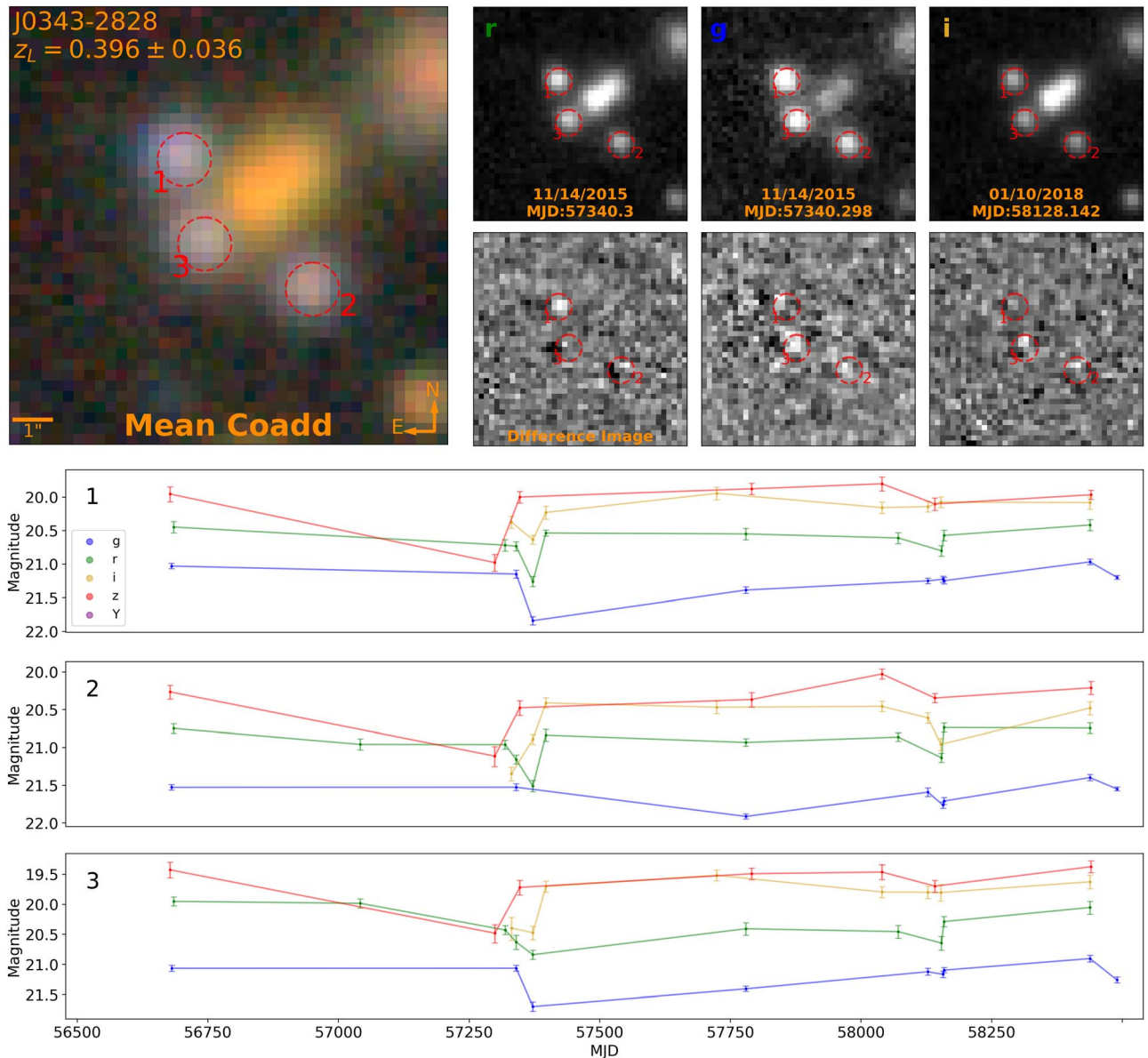


Figure 8. Lensed quasar candidate J0343-2828 (see caption of Figure 4 for the full description of each subplot).

In regard to the second point, the spectrum (Figure 15 of Lemon et al. 2023) was observed using the European Southern Observatory (ESO) Faint Object Spectrograph and Camera version 2. Indeed, the spectrum presented from 3650–8000 Å observed wavelength is relatively flat and displays no distinct QSO emission lines. We note that its signal-to-noise ratio is comparatively lower than other spectra presented in the paper.

By aggregating the information at hand (variability, HST imaging/modeling, and spectroscopy), we propose that this system could be a more exotic type of lensed quasar.¹⁴ One such possibility is a changing-look quasar that can exhibit disappearing broad emission lines (MacLeod et al. 2019; Potts & Villforth 2021; Green et al. 2022). Another possibility is that of a low-ionization broad-absorption-line quasar, where the broad emission lines may not be very obvious (Schulze et al. 2017; Leighly et al. 2018, 2019; Wethers et al. 2020). In summary, from the variability and other evidence presented, we

believe it is appropriate to reopen the discussion around J0343-2828 and reclassify it as a lensed quasar candidate. We emphasize that this reconsideration is made possible through the variability search method presented in this work.

5. Conclusion

Using our transient search pipeline, we perform a targeted search on 5807 strong-lens candidate systems and identify 7 previously confirmed lensed quasars, 3 new quadruply lensed, and 10 new doubly lensed quasar candidates. We also provide additional variability confirmation to 13 lensed quasar candidates previously identified by D23 and H23. We again stress that this does not in any way imply that the candidates presented by D23 and H23 but not presented in this paper are not lensed quasars, and acknowledge that the 13 shown in this work is likely highly incomplete to the lensed quasar candidate initial sample (see Sections 4 and 4.2). The lensed source of J0343-2828 (one of these 13 systems) was previously considered to be disconfirmed

¹⁴ Through private communications with C. Lemon and T. Schmidt.

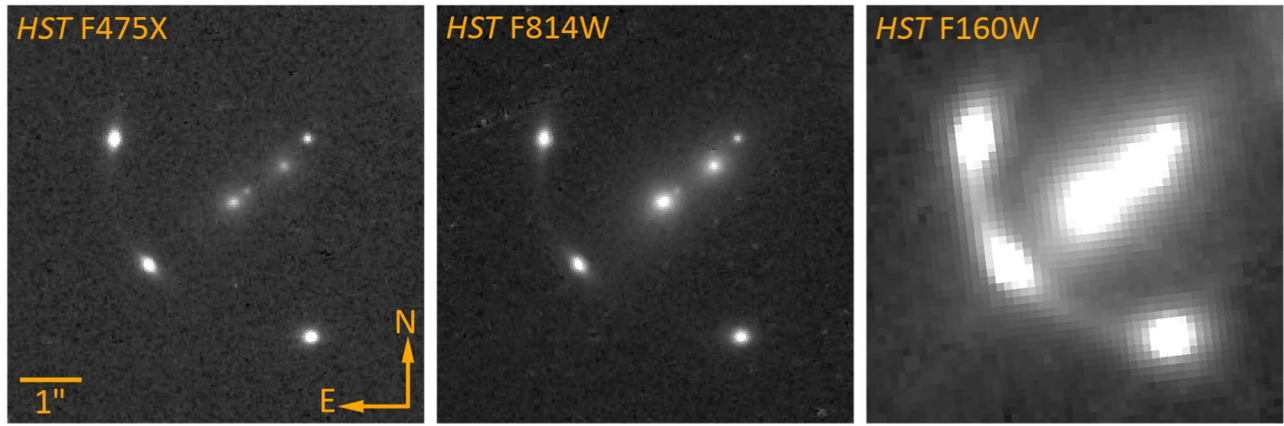


Figure 9. HST imaging of J0343-2828, in the F475X, F814W, and F160W bands (Prop ID: 15652; PI: T. Treu).

as a quasar (Lemon et al. 2023). Now with additional variability evidence, we reclassify J0343-2828 as a lensed quasar candidate.

Our pipeline, rather than just relying on potential lensed image positions, morphology, and colors, also assesses each image’s variability, allowing us to find new candidates not discovered by other lensed quasar search pipelines. With follow-up spectroscopy, it becomes possible to properly assess the correctness and completeness of our results, but we nevertheless believe these results demonstrate the promising viability of our pipeline and its applicability to future surveys such as the Vera C. Rubin Observatory Legacy Survey of Space and Time and the Nancy Grace Roman Space Telescope. As Section 4.1.2 demonstrates, applying our pipeline to future searches (with improved depth and cadence; e.g., Suyu et al. 2020) will discover new lensed quasar candidates, when supplied with a set of strong-lens candidates in the survey footprint. Furthermore, Section 4.2 shows that our methodology will allow us to give additional variability confirmation for lensed quasar candidates identified by more traditional lensed quasar search methods. From discovery to confirmation, we expect our pipeline to give a high yield in future lensed quasar searches, and with this, contribute significantly to constraining H_0 .

Acknowledgments

This work was supported in part by the Director, Office of Science, Office of High Energy Physics of the US Department of Energy under contract No. DE-AC025CH11231. This research used resources of the National Energy Research Scientific Computing Center (NERSC), a U.S. Department of Energy Office of Science User Facility operated under the same contract as above and the Computational HEP program in The Department of Energy’s Science Office of High Energy Physics provided resources through the “Cosmology Data Repository” project (grant #KA2401022). X.H. acknowledges the University of San Francisco Faculty Development Fund. The work of A.C. is supported by NOIRLab, which is managed by the Association of Universities for Research in Astronomy (AURA) under a cooperative agreement with the National Science Foundation.

This paper is based on observations at Cerro Tololo Inter-American Observatory, National Optical Astronomy Observatory (NOAO Prop ID: 2014B-0404 with co-PIs: D. J. Schlegel and A. Dey; NOAO Prop IDs: 2022A-388025 and 2022B-297190 with co-PIs: A. Palmese and L. Wang), which is

operated by the Association of Universities for Research in Astronomy (AURA) under a cooperative agreement with the National Science Foundation.

This project uses data obtained with the Dark Energy Camera, which was constructed by the Dark Energy Survey collaboration. Funding for the DES Projects has been provided by the U.S. Department of Energy, the U.S. National Science Foundation, the Ministry of Science and Education of Spain, the Science and Technology Facilities Council of the United Kingdom, the Higher Education Funding Council for England, the National Center for Supercomputing Applications at the University of Illinois at Urbana-Champaign, the Kavli Institute of Cosmological Physics at the University of Chicago, the Center for Cosmology and Astro-Particle Physics at the Ohio State University, the Mitchell Institute for Fundamental Physics and Astronomy at Texas A&M University, Financiadora de Estudos e Projetos, Fundação Carlos Chagas Filho de Amparo à Pesquisa do Estado do Rio de Janeiro, Conselho Nacional de Desenvolvimento Científico e Tecnológico and the Ministério da Ciência, Tecnologia e Inovação, the Deutsche Forschungsgemeinschaft, and the Collaborating Institutions in the Dark Energy Survey. The Collaborating Institutions are Argonne National Laboratory, the University of California at Santa Cruz, the University of Cambridge, Centro de Investigaciones Energéticas, Medioambientales y Tecnológicas-Madrid, the University of Chicago, University College London, the DES-Brazil Consortium, the University of Edinburgh, the Eidgenössische Technische Hochschule (ETH) Zürich, Fermi National Accelerator Laboratory, the University of Illinois at Urbana-Champaign, the Institut de Ciències de l’Espai (IEEC/CSIC), the Institut de Física d’Altes Energies, Lawrence Berkeley National Laboratory, the Ludwig-Maximilians Universität München and the associated Excellence Cluster Universe, the University of Michigan, the National Optical Astronomy Observatory, the University of Nottingham, the Ohio State University, the OzDES Membership Consortium the University of Pennsylvania, the University of Portsmouth, SLAC National Accelerator Laboratory, Stanford University, the University of Sussex, and Texas A&M University.

We thank the referee and data editor for the insightful comments on reorganizing and improving the quality of our paper. We also thank C. Lemon and T. Schmidt for cross-referencing our candidates with catalogs of previously identified lensed quasar candidates, and for thought-provoking discussions regarding J0343-2828.

Software: Astropy (Astropy Collaboration et al. 2013, 2018), Montage (Jacob et al. 2010), SEP (Bertin & Arnouts 1996; Barbary 2018), SNCosmo (Barbary 2014), NumPy (Harris et al. 2020), Matplotlib (Hunter 2007).

Appendix A Lensed Quasar Candidates from Targeted Search

Here, we present the candidate systems identified by our first targeted search on strong-lens candidates, shown in Figure 3 (with the exception of WG021416.37-210535.3 and DESI-350.3458-03.5082, which are presented in Section 4.1.1 and Section 4.1.2, respectively).

A.1. Previously Identified Lensed Quasars

DESJ0340-2545—This system is a quadruply lensed quasar (Figure A1), discovered and spectroscopically confirmed by Lemon et al. (2020). This system was “rediscovered” in SLS II as a strong-lens candidate, and therefore it was included in our search. We subsequently found that this is a known system. Unlike most other systems presented, this is likely a cluster-lens lensed quasar system, with three visibly resolved images north, west, and southwest of the main lensing galaxy, respectively.

SDSS J2222+2745—This system is a sextuply lensed quasar (Figure A1.2), discovered and spectroscopically confirmed by Dahle et al. (2013). This system was “rediscovered” in SLS II as a strong-lens candidate, and therefore it was included in our search. We subsequently found that this is a known system. Light curves of this system were shown in Dahle et al. (2015). In Figure A1.2, there are three identifiable images in the Legacy Imaging Surveys, and the remaining three are too faint and/or too close to the cluster center. The bright PSF-like object south of the cluster lens has been spectroscopically confirmed to be a white dwarf (Dahle et al. 2013).

KIDSJ0008-3237—This system is a quadruply lensed quasar (Figure A1.3), initially discovered as a lensed quasar candidate by Khramtsov et al. (2019). This system was identified in SLS III as a strong-lens candidate, and therefore it was included in our search. We subsequently found that this is a known lensed quasar candidate. We posit that the “image” on the southwest of the lens is the result of two lensed quasar images merging, with two other images seen east and northwest of the lens.

J0011-0845—This system is a doubly lensed quasar (Figure A1.4), initially identified and spectroscopically confirmed by Lemon et al. (2018b), but no light curves were provided. This system was “rediscovered” in SLS III as a strong-lens candidate, and therefore it was included in our search. We subsequently found that this is a known system. Though this system was previously discovered, we show new light curves for this system. This system exhibits a typical doubly lensed quasar morphology, with two bright, PSF-like images on directly opposite sides of a posited lens galaxy.

J0030-3358—This system is a doubly lensed quasar (Figure A1.5), initially identified as a strong-lens candidate in SLS II. It was later spectroscopically confirmed as a lensed quasar in Lemon et al. (2023), though no light curves have been provided. Though J0030-3358 exhibits a double structure, the image-to-lens angular separations of the two images clearly differ, and the southern image is significantly brighter than the northern image, which may indicate a longer time delay (as a

strong difference in magnification implies a larger $\Delta\kappa$ and hence gravitational time delay between images). Also similarly, both images are bright, blue, PSF-like, and variable.

HSCJ091843.38-022007.3—This system is a doubly lensed quasar (Figure A1.6), initially identified as a strong-lens candidate in Sonnenfeld et al. (2020). It was later spectroscopically confirmed as a lensed quasar in Jaelani et al. (2021), but no light curves have been provided. This system shares a similar structure to J0030-3358 (see Figure A1.3), as both exhibit a dim image near the lens galaxy and a brighter, more distant image on the opposite side of the lens galaxy.

A.2. New Lensed Quasar Candidates

DESI-343.6329-50.4884—This system is a quadruply lensed quasar candidate (Figure A2), initially identified as a grade A strong-lensing candidate in SLS III. With DR10 data, the Tractor only identifies three images, with a fourth one likely merging with another image. While at first glance, these systems do not have the appearance of a typical lensed quasar system, our pipeline is still able to identify PSF sources within the images; this also applies to the next system.

DESI-344.8782+01.2913—This system is a quadruply lensed quasar candidate (Figure A2.2), initially identified as a grade C strong-lensing candidate in SLS III. It is possible that the arc on the southeast of the lens galaxy is comprised of two lensed quasar images merging. The brightest posited image lies directly north of the lens. There is also a possible fourth image to the southwest of the lens.

DESI-009.5736-64.5942—This system is a doubly lensed quasar candidate (Figure A2.3), initially identified as a grade C strong-lensing candidate in SLS III. The posited lens consists of two red galaxies, with two lensed images north and west of it.

DESI-011.9124+03.3756—This system is a doubly lensed quasar candidate (Figure A2.4), initially identified as a grade A strong-lensing candidate in SLS III. This system also exhibits a double structure similar to J0011-0845 (see Figure A1.3).

DESI-033.9735-12.6841—This system is a doubly lensed quasar candidate (Figure A2.5), initially identified as a grade C strong-lensing candidate in SLS I. While this system also shares a typical double structure as the previous six candidates, DESI-033.9735-12.6841 has a significantly larger Einstein radius ($\sim 2''$).

DESI-071.8595-18.9863—This system is a doubly lensed quasar candidate (Figure A2.6), initially identified as a grade B strong-lensing candidate in SLS III. This system also exhibits a double structure similar to J0011-0845 (see Figure A1.3).

DESI-080.2447-61.8266—This system is a doubly lensed quasar candidate (Figure A2.7), initially identified as a grade C strong-lensing candidate in SLS III. This system also exhibits a double structure similar to J0011-0845 (see Figure A1.3).

DESI-089.5700-30.9485—This system is a doubly lensed quasar candidate (Figure A2.8), initially identified as a grade B strong-lensing candidate in SLS II. While there is a clear arc north of the lens galaxy, the posited lensed quasar images are located south and northeast of the lens galaxy. Hence, we posit that the lensed quasar resides in a different source galaxy than the arc, as it would be improbable for the quasar to be hosted by the arc given their separation. The posited quasar images seem to be point sources and exhibit variability between exposures. The presence of an additional source can provide degeneracy-breaking modeling constraints, allowing for tighter measurements of H_0 (e.g., Shajib et al. 2020).

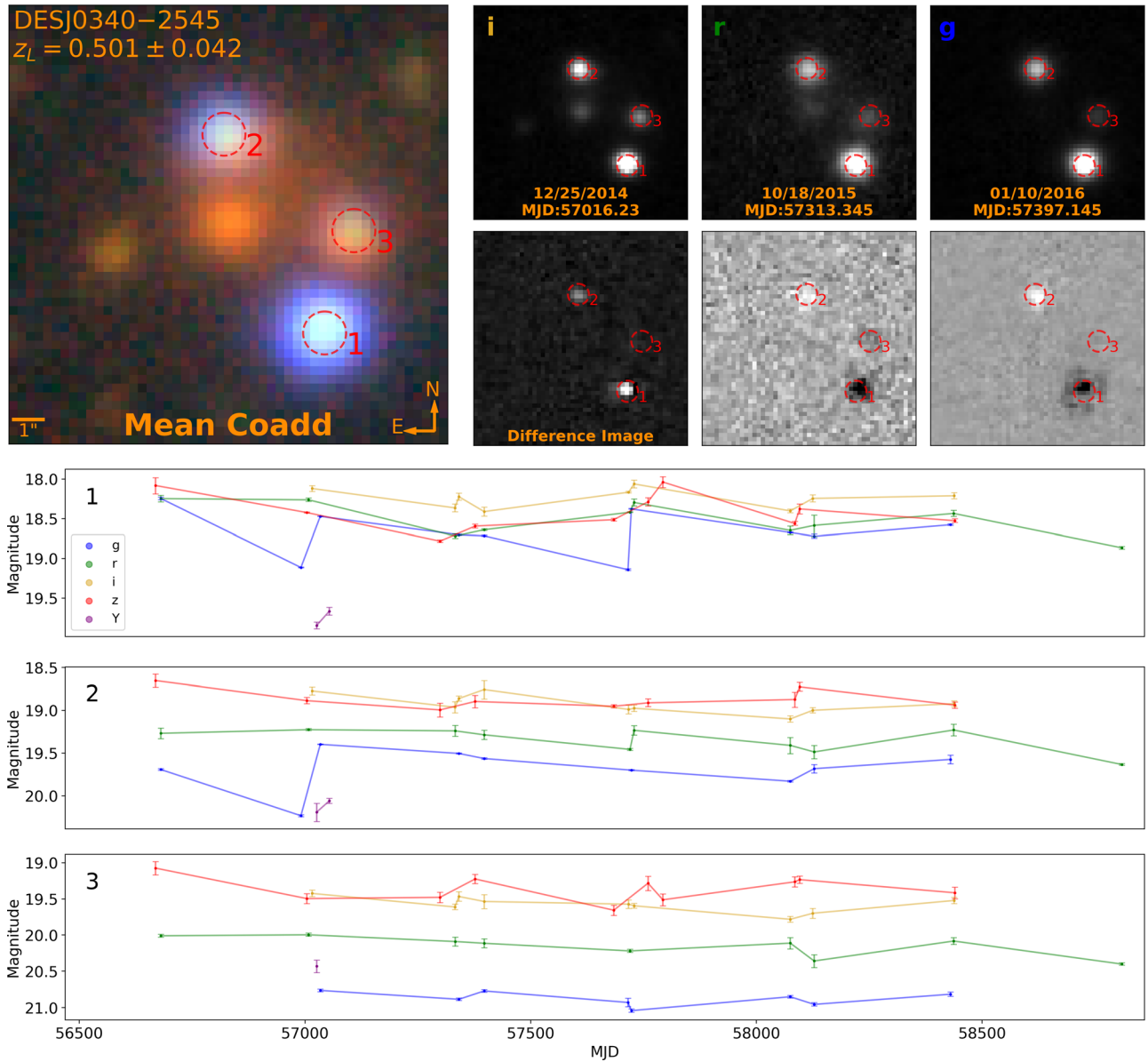


Figure A1. Lensed quasar DESJ0340-2545 (see caption of Figure 4 for the full description of each subplot). (The complete figure set (six images) is available in the [online article](#).)

DESI-308.0432-41.5946—This system is a doubly lensed quasar candidate (Figure A2.9), initially identified as a grade C strong-lensing candidate in SLS III. *DESI-308.0432-41.5946* differs somewhat from the typical double morphology, as the two posited lensed quasar images and the lens galaxy are far from collinear. Since the posited images are still PSF-shaped and variable, we consider this to be a strong lensed quasar candidate. However, the noncollinearity could possibly indicate the presence of faint and unresolved (in DECam observations) lensed quasar images (see an example in Figure 5).

DESI-316.8445-00.9920—This system is a doubly lensed quasar candidate (Figure A2.10), initially identified as a grade B strong-lensing candidate in SLS II. This system also exhibits a double structure similar to J0011-0845 (see Figure A1.3).

DESI-324.5771-56.6459—This system is a doubly lensed quasar candidate (Figure A2.11), initially identified as a grade C strong-lensing candidate in SLS III. As with the previous system, *DESI-308.0432-41.5946* appears to be a double. However, given the notable noncollinearity, there may be other lensed images too faint and/or too close to the lens.

DESI-012.3074-25.6429—This system is a doubly lensed quasar candidate (Figure A2.12), initially identified as a grade C strong-lensing candidate in SLS III. While only one variable image (directly east of the lens) is visible, given the observed configuration, this candidate system may have a counterimage on the opposite side of the lens. If so, such an image would likely be demagnified and would be overwhelmed by the lens galaxy light.

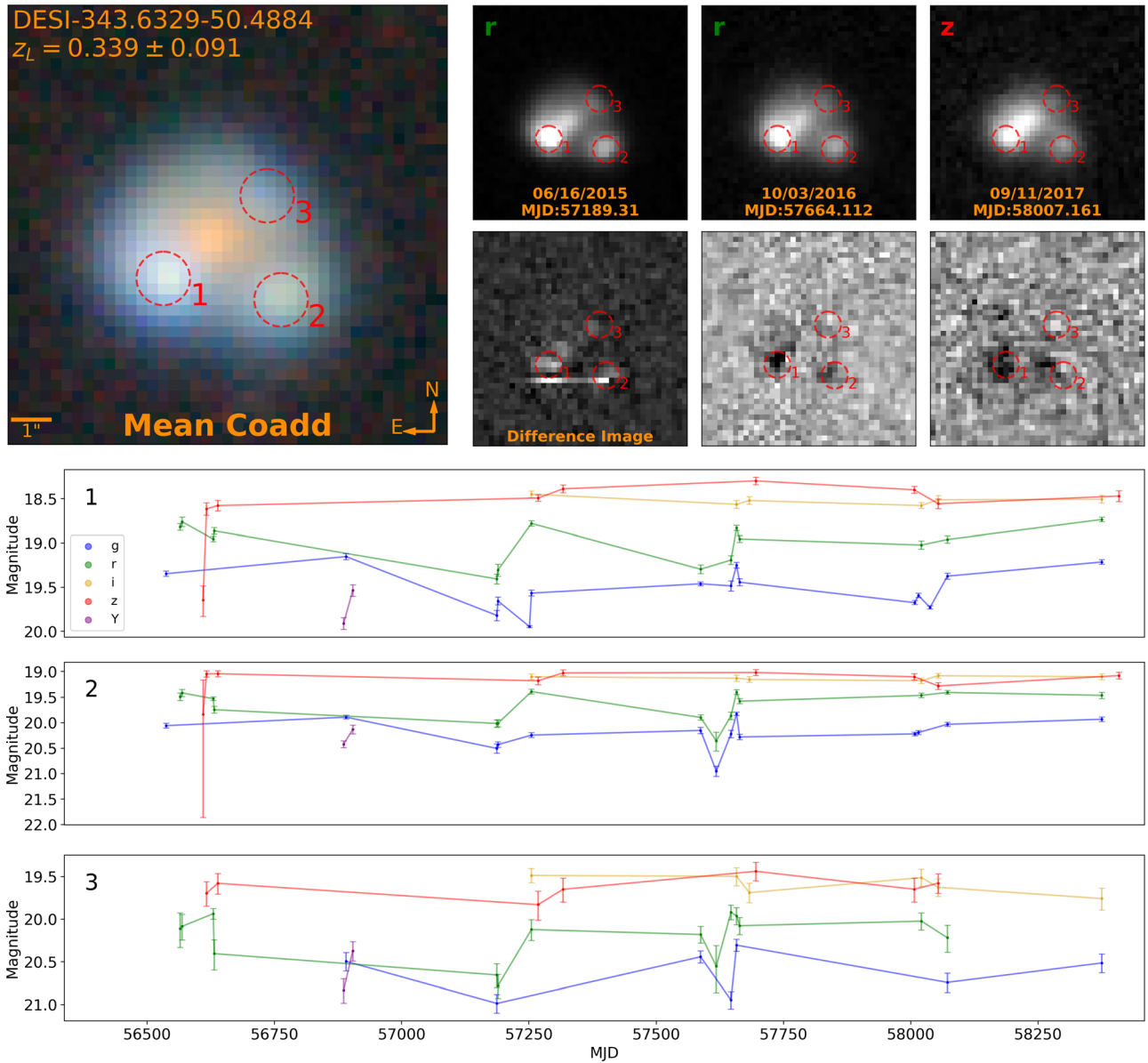


Figure A2. Lensed quasar DESI-343.6329-50.4884 (see caption of Figure 4 for the full description of each subplot). (The complete figure set (12 images) is available in the [online article](#).)

Appendix B Variability Confirmation of Previously Discovered Lensed Quasar Candidates

Here, we present the systems identified by our second targeted search on strong lensed quasar candidates, shown in Figure 7 (with the exception of J0343-2828, which is presented in Section 4.2).

DESI-011.5839-26.1241—This system is a doubly lensed quasar candidate (Figure B1), initially classified as a grade B in both D23 and H23. This system exhibits a typical doubly lensed quasar structure, with the lens galaxy likely overwhelmed by the lensed quasar light.

DESI-029.1039-27.8562—This system is a doubly lensed quasar candidate (Figure B1.2), initially classified as a grade A in both D23 and H23. This system, like all the following systems, exhibits the characteristic doubly lensed quasar structure (see Figure A1.3). In DESI-029.1039-27.8562, we

can identify the lens galaxy (the red galaxy between the two lensed images), but this is not always possible as the lensed quasar image can sometimes overwhelm the lens galaxy.

DESI-030.0872-15.1609—This system is a doubly lensed quasar candidate (Figure B1.3), initially classified as a grade A in D23. This system also exhibits the characteristic doubly lensed quasar structure, but the lens galaxy cannot be discerned; it is likely that the quasar light overwhelms the lens galaxy light.

DESI-038.0655-24.4942—This system is a doubly lensed quasar candidate (Figure B1.4), initially classified as a grade A in both D23 and H23. This system exhibits a typical doubly lensed quasar structure, with the lens galaxy likely overwhelmed by the lensed quasar light. The two images are debled by the Tractor, despite being very close to one another.

DESI-040.6886-10.0492—This system is a doubly lensed quasar candidate (Figure B1.5), initially classified as a grade C in D23 and a grade A in H23. This system exhibits a typical

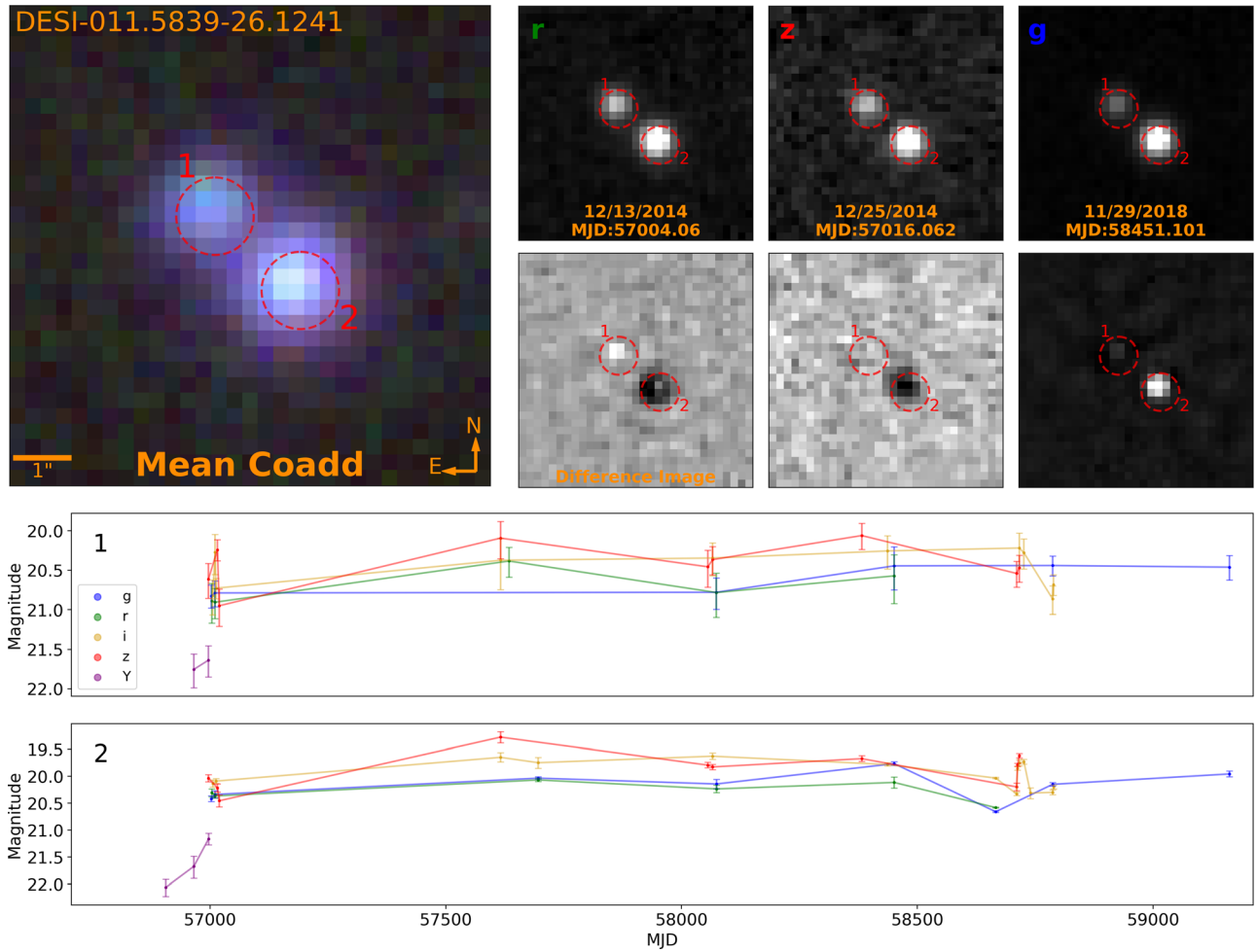


Figure B1. Lensed quasar DESI-011.5839-26.1241 (see caption of Figure 4 for the full description of each subplot). (The complete figure set (12 images) is available in the [online article](#).)

doubly lensed quasar structure, with the lens galaxy likely overwhelmed by the lensed quasar light.

DESI-060.4504-25.2439—This system is a doubly lensed quasar candidate (Figure B1.6), initially classified as a grade A in D23. The lens galaxy is visible as a bright red galaxy between two lensed images in this double structure.

DESI-076.5562-25.5135—This system is a doubly lensed quasar candidate (Figure B1.7), initially classified as a grade B in both D23 and H23. This system exhibits a typical doubly lensed quasar structure, with the lens galaxy likely overwhelmed by the lensed quasar light.

DESI-202.0009-07.8030—This system is a doubly lensed quasar candidate (Figure B1.8), initially classified as a grade A in both D23 and H23. This system exhibits a typical doubly lensed quasar structure, with the lens galaxy likely overwhelmed by the lensed quasar light.

DESI-306.7073-42.4719—This system is a doubly lensed quasar candidate (Figure B1.9), initially classified as a grade B in D23. This system exhibits a typical doubly lensed quasar structure, with the lens galaxy likely overwhelmed by the lensed quasar light. The two images are debled by the Tractor, despite being very close to one another.

DESI-325.8843+12.5745—This system is a doubly lensed quasar candidate (Figure B1.10), initially classified as a grade

C in D23 and a grade A in H23. This system exhibits a typical doubly lensed quasar structure, with the lens galaxy likely overwhelmed by the lensed quasar light. The two images are debled by the Tractor, despite being very close to one another.

DESI-345.6309-41.9157—This system is a doubly lensed quasar candidate (Figure B1.11), initially classified as a grade C in D23 and a grade A in H23. This system exhibits a typical doubly lensed quasar structure, with the lens galaxy likely overwhelmed by the lensed quasar light.

DESI-346.9550-49.2117—This system is a doubly lensed quasar candidate (Figure B1.12), initially classified as a grade B in D23. This system exhibits a typical doubly lensed quasar structure, with the lens galaxy likely overwhelmed by the lensed quasar light.

ORCID iDs

William Sheu <https://orcid.org/0000-0003-1889-0227>
 Xiaosheng Huang <https://orcid.org/0000-0001-8156-0330>
 Aleksandar Cikota <https://orcid.org/0000-0001-7101-9831>
 Nao Suzuki <https://orcid.org/0000-0001-7266-930X>
 Antonella Palmese <https://orcid.org/0000-0002-6011-0530>
 David J. Schlegel <https://orcid.org/0000-0002-5042-5088>
 Christopher Storfer <https://orcid.org/0000-0002-0385-0014>

References

- Agnello, A. 2018, *RNAAS*, **2**, 42
- Agnello, A., Lin, H., Kuropatkin, N., et al. 2018, *MNRAS*, **479**, 4345
- Astropy Collaboration, Price-Whelan, A. M., Sipőcz, B. M., et al. 2018, *AJ*, **156**, 123
- Astropy Collaboration, Robitaille, T. P., Tollerud, E. J., et al. 2013, *A&A*, **558**, A33
- Barbary, K. 2014, *sncosmo* v0.4.2, Zenodo, doi:10.5281/zenodo.11938
- Barbary, K. 2018, SEP: Source Extraction and Photometry, Astrophysics Source Code Library, ascl:1811.004
- Bertin, E., & Arnouts, S. 1996, *A&AS*, **117**, 393
- Bramich, D. M. 2008, *MNRAS*, **386**, L77
- Carrasco, M., Barrientos, L. F., Anguita, T., et al. 2017, *yCat, J/ApJ/834/210*
- Chen, W., Kelly, P. L., Oguri, M., et al. 2022, *Natur*, **611**, 256
- Dahle, H., Gladders, M. D., Sharon, K., Bayliss, M. B., & Rigby, J. R. 2015, *ApJ*, **813**, 67
- Dahle, H., Gladders, M. D., Sharon, K., et al. 2013, *ApJ*, **773**, 146
- Dawes, C., Storfer, C., Huang, X., et al. 2023, *ApJS*, **269**, 61
- DESI Collaboration, Aghamousa, A., Aguilar, J., et al. 2016, arXiv:1611.00036
- Dey, A., Schlegel, D. J., Lang, D., et al. 2019, *AJ*, **157**, 168
- Diehl, H. T., Buckley-Geer, E. J., Lindgren, K. A., et al. 2017, *ApJS*, **232**, 15
- Dux, F., Lemon, C., Courbin, F., et al. 2023, *A&A*, **682**, A47
- Fawcett, V. A., Alexander, D. M., Rosario, D. J., et al. 2020, *MNRAS*, **494**, 4802
- Flaugher, B., Diehl, H. T., Honscheid, K., et al. 2015, *AJ*, **150**, 150
- Freedman, W. L. 2021, *ApJ*, **919**, 16
- Frye, B., Pascale, M., Cohen, S., et al. 2023, *TNSAN*, **96**, 1
- Goobar, A., Amanullah, R., Kulkarni, S. R., et al. 2017, *Sci*, **356**, 291
- Goobar, A., Johansson, J., Dhawan, S., et al. 2022, *TNSAN*, **180**, 1
- Green, P. J., Pulgarin-Duque, L., Anderson, S. F., et al. 2022, *ApJ*, **933**, 180
- Harris, C. R., Millman, K. J., van der Walt, S. J., et al. 2020, *Natur*, **585**, 357
- He, Z., Li, N., Cao, X., et al. 2023, *A&A*, **672**, A123
- Hu, L., Wang, L., Chen, X., & Yang, J. 2022, *ApJ*, **936**, 157
- Huang, X., Storfer, C., Ravi, V., et al. 2020, *ApJ*, **894**, 78
- Huang, X., Storfer, C., Gu, A., et al. 2021, *ApJ*, **909**, 27
- Hunter, J. D. 2007, *CSE*, **9**, 90
- Inada, N., Oguri, M., Shin, M.-S., et al. 2012, *AJ*, **143**, 119
- Jacob, J. C., Katz, D. S., Berriman, G. B., et al. 2010, arXiv:1005.4454
- Jacobs, C., Glazebrook, K., Collett, T., More, A., & McCarthy, C. 2017, *MNRAS*, **471**, 167
- Jacobs, C., Collett, T., Glazebrook, K., et al. 2019, *ApJS*, **243**, 17
- Jaelani, A. T., Rusu, C. E., Kayo, I., et al. 2021, *MNRAS*, **502**, 1487
- Kelly, B. C., Treu, T., Malkan, M., Pancoast, A., & Woo, J.-H. 2013, *ApJ*, **779**, 187
- Kelly, P., Zitrin, A., Oguri, M., et al. 2022, *TNSAN*, **169**, 1
- Kelly, P. L., Rodney, S. A., Treu, T., et al. 2015, *Sci*, **347**, 1123
- Kelly, P. L., Rodney, S., Treu, T., et al. 2023, *Sci*, **380**, abh1322
- Khrantsov, V., Sergeev, A., Spiniello, C., et al. 2019, *A&A*, **632**, A56
- Kochanek, C. S., Mochejska, B., Morgan, N. D., & Stanek, K. Z. 2006, *ApJL*, **637**, L73
- Kostrzewa-Rutkowska, Z., Kozłowski, S., Lemon, C., et al. 2018, *MNRAS*, **476**, 663
- Lacki, B. C., Kochanek, C. S., Stanek, K. Z., Inada, N., & Oguri, M. 2009, *ApJ*, **698**, 428
- Lang, D., Hogg, D. W., & Mykytyn, D. 2016, The Tractor: Probabilistic astronomical source detection and measurement, Astrophysics Source Code Library, ascl:1604.008
- Leighly, K. M., Terndrup, D. M., Gallagher, S. C., Richards, G. T., & Dietrich, M. 2018, *ApJ*, **866**, 7
- Leighly, K. M., Terndrup, D. M., Lucy, A. B., et al. 2019, *ApJ*, **879**, 27
- Lemon, C., Auger, M. W., McMahon, R., et al. 2020, *MNRAS*, **494**, 3491
- Lemon, C., Anguita, T., Auger-Williams, M. W., et al. 2023, *MNRAS*, **520**, 3305
- Lemon, C. A., Auger, M. W., & McMahon, R. G. 2018a, *MNRAS*, **483**, 4242
- Lemon, C. A., Auger, M. W., McMahon, R. G., & Ostrovski, F. 2018b, *MNRAS*, **479**, 5060
- Liao, K. 2019, *ApJ*, **871**, 113
- MacLeod, C. L., Green, P. J., Anderson, S. F., et al. 2019, *ApJ*, **874**, 8
- More, A., Oguri, M., Kayo, I., et al. 2015, *MNRAS*, **456**, 1595
- Moustakas, L. 2012, in 10th Hellenic Astronomical Conf., ed. I. Papadakis & A. Anastasiadis, **14**
- Planck Collaboration, Aghanim, N., Akrami, Y., et al. 2020, *A&A*, **641**, A6
- Potts, B., & Villforth, C. 2021, *A&A*, **650**, A33
- Pourrahmani, M., Nayyeri, H., & Cooray, A. 2018, *ApJ*, **856**, 68
- Quimby, R. M., Oguri, M., More, A., et al. 2014, *Sci*, **344**, 396
- Riess, A. G., Yuan, W., Macri, L. M., et al. 2022, *ApJL*, **934**, L7
- Rodney, S. A., Brammer, G. B., Pierel, J. D. R., et al. 2021, *NatAs*, **5**, 1118
- Schmidt, T., Treu, T., Birrer, S., et al. 2023, *MNRAS*, **518**, 1260
- Schulze, A., Schramm, M., Zuo, W., et al. 2017, *ApJ*, **848**, 104
- Shajib, A. J., Birrer, S., Treu, T., et al. 2020, *MNRAS*, **494**, 6072
- Shajib, A. J., Mozumdar, P., Chen, G. C.-F., et al. 2023, *A&A*, **673**, A9
- Sheu, W., Huang, X., Cikota, A., et al. 2023, *ApJ*, **952**, 10
- Sonnenfeld, A., & Leauthaud, A. 2018, *MNRAS*, **477**, 5460
- Sonnenfeld, A., Verma, A., More, A., et al. 2020, *A&A*, **642**, A148
- Storfer, C., Huang, X., Gu, A., et al. 2022, arXiv:2206.02764
- Suyu, S. H., Huber, S., Cañameras, R., et al. 2020, *A&A*, **644**, A162
- Walsh, D., Carswell, R. F., & Weymann, R. J. 1979, *Natur*, **279**, 381
- Wethers, C. F., Kotilainen, J., Schramm, M., & Schulze, A. 2020, *MNRAS*, **498**, 1469
- Weymann, R. J., Chaffee, F. H. J., Davis, M., et al. 1979, *ApJL*, **233**, L43
- Weymann, R. J., Latham, D., Angel, J. R. P., et al. 1980, *Natur*, **285**, 641
- Wong, K. C., Sonnenfeld, A., Chan, J. H. H., et al. 2018, *ApJ*, **867**, 107
- Wong, K. C., Suyu, S. H., Chen, G. C.-F., et al. 2019, *MNRAS*, **498**, 1420
- Zhou, R., Newman, J. A., Mao, Y.-Y., et al. 2020, *MNRAS*, **501**, 3309